Designer Variable Repeat Length Polypeptides as Scaffolds for Surface Immobilization of Quantum Dots

Igor L. Medintz,*,† Kim E. Sapsford,†,‡ Aaron R. Clapp,§ Thomas Pons,§,|| Seiichiro Higashiya,⊥ John T. Welch,⊥ and Hedi Mattoussi*,§

Center for Bio/Molecular Science and Engineering, Code 6900, and Division of Optical Sciences, Code 5611, U.S. Naval Research Laboratory, Washington, D.C. 20375, George Mason University, 10910 University Boulevard, MS 4E3, Manassas, Virginia 20110, Chemical and Biomolecular Engineering Department, Johns Hopkins University, Baltimore, Maryland 21218, and Department of Chemistry, The University of Albany, SUNY, 1400 Washington Avenue, Albany, New York 12222

Received: January 28, 2006; In Final Form: March 27, 2006

We demonstrate the use of a series of engineered, variable-length *de novo* polypeptides to discretely immobilize luminescent semiconductor nanocrystals or quantum dots (QDs) onto functional surfaces. The polypeptides express N-terminal dicysteine and C-terminal hexahistidine residues that flank a variable number (1, 3, 5, 7, 14, 21, 28, or 35) of core β-strand repeats, with tyrosine, glutamic acid, histidine, and lysine residues located at the turns. Polypeptides have molecular weights ranging from 4 to 83 kDa and retain a rigid structure based on the antiparallel β-sheet motif. We first use a series of dye-labeled polypeptides to test and characterize their self-assembly onto hydrophilic CdSe−ZnS QDs using fluorescence resonance energy transfer (FRET). Results indicate that peptides maintain their β-sheet conformation after self-assembly onto the QD surfaces, regardless of their length. We then immobilize biotinylated derivatives of these polypeptides on a NeutrAvidin-functionalized substrate and use them to capture QDs via specific interactions between the peptides' polyhistidine residues and the nanocrystal surface. We found that each of the polypeptides was able to efficiently capture QDs, with a clear correlation between the density of the surface-tethered peptide and the capacity for nanocrystal capture. The versatility of this capture strategy is highlighted by the creation of a variety of one- and two-dimensional polypeptide−QD structures as well as a self-assembled surface-immobilized FRET-based nutrient sensor.

Introduction

Metallic nanoparticles and semiconductor nanocrystals or quantum dots (QDs) are among a new generation of nanomaterials with projected utility in sensors, light emitting and light harvesting devices, and molecular electronics, as well as biomedical imaging.[1−7] Many of these applications will ultimately require intimate control over the surface functionalities of these materials and the ability to array them on various substrates. Different strategies have been proposed, either individually or in combination, for creating surface-ordered arrays of QDs and other nanoparticles. These include deposition of nanoparticles dispersed in diblock-copolymer templates,[8] using capillary forces for immobilization,[9] self-assemblies driven by electrostatic and hydrogen bond interactions,[8,10] microcontact printing,[11,12] and capture of hydrophilic nanocrystals by protein-coated substrates.[13−17] The most effective strategy should allow immobilization of discrete arrays of nanoparticles, control over their density, and the ability to attach additional materials/functionalities to these arrays as desired. Protein and peptide-driven assembly is one route that can potentially accomplish some of these goals due to the availability of recombinant design and engineering techniques.[18] Furthermore, the intrinsic structural, self-assembly, order, and scaffolding properties of proteins are accompanied by the added benefit of displaying specific chemical functionalities on the protein surface. For example, engineering thiol or amino functionalities at desired locations within the protein sequence can provide sites for further chemical modification.[18] Proteins and polypeptides can also be engineered to assume particular structures such as α-helices or β-sheets.

In this report, we use metal-affinity-driven self-assembly to conjugate *de novo* designer, variable-repeat-length β-strand polypeptides to luminescent QDs. This is accomplished by using the polypeptide N-terminal hexahistidine interaction with the QD surface. The polypeptide conformation in the conjugates is derived by using fluorescence resonance energy transfer (FRET) between the centrally located QD donor and dyes attached to the polypeptides. We further demonstrate the use of these polypeptides to discretely capture/immobilize QDs on surfaces. We then highlight the versatility of this immobilization strategy by creating surface-tethered arrays of luminescent QDs and a FRET-based QD-biosensing assembly.

Experimental Section

Materials. Monofunctional maleimide Cy3 dye and rhodamine red (RR) maleimide were purchased from Amersham Bio-

* To whom correspondence should be addressed. Phone: 202-404-6046 (I.L.M.); 202-767-9473 (H.M.). Fax: 202-767-9594 (I.L.M.); 202-404-8114 (H.M.). E-mail: Imedintz@cbmse.nrl.navy.mil (I.L.M.); Hedimat@ccs.nrl.navy.mil (H.M.).

† Center for Bio/Molecular Science and Engineering, U.S. Naval Research Laboratory.

‡ George Mason University.

§ Division of Optical Sciences, U.S. Naval Research Laboratory.

|| Johns Hopkins University.

⊥ The University of Albany, SUNY.

10.1021/jp060611z CCC: $33.50
Published on Web 05/17/2006

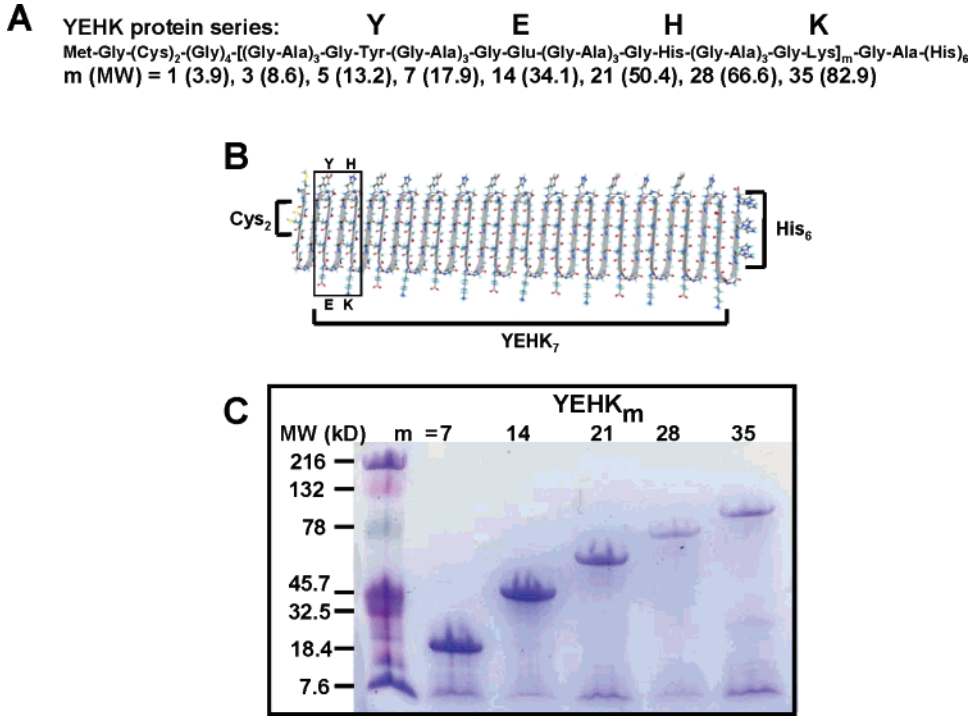

Figure 1. (A) Amino acid sequence of the repetitive polypeptide $YEHK_m$ protein series used with predicted molecular weights in parentheses. The $[\ ]_m$ designates the core repeat unit. (B) Schematic structure of the $Cys_2-YEHK_7-His_6$ polypeptide in a β-strand conformation with a single YEHK repeat boxed. (C) SDS−PAGE gel of the purified $Cys_2-YEHK_m-His_6$ protein series where $m = 7$, 14, 21, 28, or 35.

sciences (Piscataway, NJ) and Molecular Probes (Eugene, OR), respectively. High binding capacity 96-well microtiter plates coated with Reacti-Bind NeutrAvidin and EZ-link poly(ethylene oxide) (PEO)−maleimide−biotin were purchased from Pierce (Rockford, IL). Polyallylamine hydrochloride (PAH) was purchased from Polysciences, Inc. (Warrington, PA). Flow cells used for patterning were prepared using poly(dimethylsiloxane) (PDMS) molds (Nusil Silicone Technology; Carpintera, CA). Cadmium, zinc, selenium, and sulfur precursors for QD synthesis were purchased from Strem Chemicals (Newburyport, MA) and Aldrich (St Louis, MO). Thiotic acid was purchased from Aldrich and modified through a reduction reaction to dihydrolipoic acid (DHLA).[19]

Hydrophilic QDs. CdSe−ZnS core−shell QDs were synthesized using a stepwise reaction from organometallic precursors following well-established synthetic routes.[20,21] QDs were then rendered water-soluble via cap exchange of the native ligands with dihydrolipoic acid (DHLA).[19] Figure 2 shows the absorption and photoluminescence (PL) spectra for the QDs and dyes used in this study.

Peptide and Protein Expression and Purification. The DNA coding sequences for the polypeptides were constructed using recursive oligomerization and block copolymerization of repetitive units. Synthetic oligonucleotides encoding the initial repeat units were ligated together and cloned into plasmid vectors and appropriate repeat numbers selected for by PCR. Additional details can be found in refs 22−27. The series of peptide genes used in this study were subcloned into pET28 expression vectors (Novagen, San Diego, CA) and expressed in BLR(DE3)pLysSRARE *Escherichia coli* (*E. coli*) host cells (Novagen).[22,23] Cells were grown in 25 μg/mL kanamycin and 34 μg/mL chloramphenicol, and expression was induced with 1 mM isopropyl-β-D-thiogalactopyranoside (IPTG) for 4 h. Cells were harvested by centrifugation and lysed by boiling for 1 h in denaturing buffer (100 mM NaH_2PO_4, 10 mM Tris, 6 M guanidine HCl, 5 mM imidazole, 10 mM 2-mercaptoethanol, pH 8). After centrifugation, the peptide present in the soluble lysate was purified using Ni−NTA affinity chromatography as

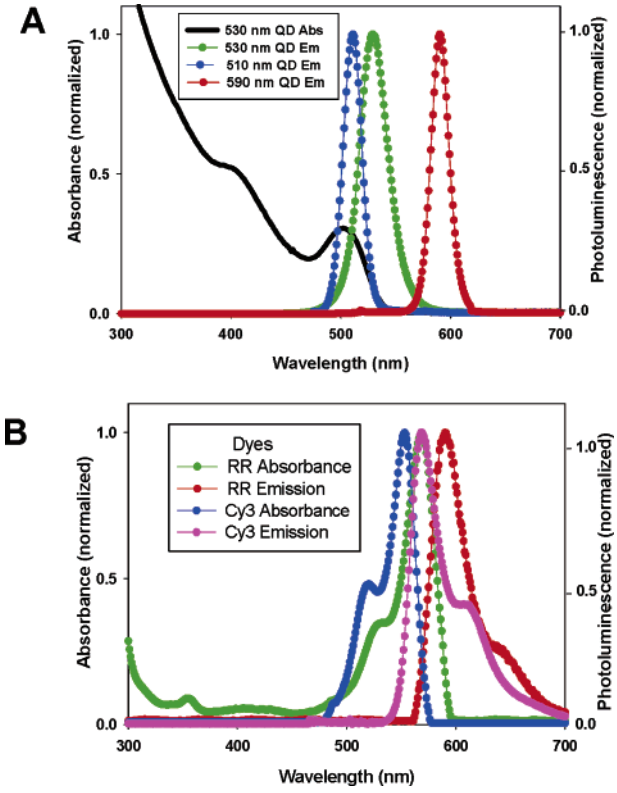

Figure 2. (A) Normalized absorption for 530 and PL emission spectra of 510, 530, and 590 nm emitting QDs. (B) Absorption and emission spectra of rhodamine red (RR) and $YEHK_7$−Cy3. (Quantum yields: 0.13 for 510 nm QDs, 0.15 for 530 nm QDs, and 0.20 for 590 nm QDs).

described.[28] Peptide concentration was determined from the optical density (OD) at 280 nm using UV spectroscopy. Typical yields were ≥100 mg/L of culture. Peptides were subsequently labeled with Cy3 or RR or modified with biotin using standard procedures.[15,29−31] A dye-to-peptide labeling ratio of ∼2, derived by monitoring the absorptions of the peptide at 280 nm and the dye at its absorption maxima, was consistent with the presence of 2 cysteines per peptide. Maltose binding protein (MBP) mutagenesis, expression in *E. coli* host cells, purification using Ni−NTA affinity chromatography, and dye-labeling was carried out as described.[28,30,31]

Characterization of QD-YEHK$_m$ Assemblies in Solution. Solutions of QD-peptide conjugates used for FRET characterization were prepared by mixing 10 nM of QDs in borate buffer (QDs emitting at 510 and 530 nm were used) with appropriate peptides at an increasing ratio of Cy3-labeled to unlabeled YEHK$_m$ while maintaining the total number of peptides per QD-conjugate constant at ∼20.[30−32] Figure 3A shows a schematic representation of a QD−peptide conjugate engaged in FRET interactions. After 1 h incubation, emission spectra were collected using a Safire dual monochromator multifunction microtiter plate reader (Tecan, Boston, MA) with 300 nm excitation. Estimates of the center-to-center donor−acceptor separation distances r were derived by fitting the experimental data from the FRET efficiencies E using the following expression:[31,32]

$$r_n = \left(\frac{n(1-E)}{E}\right)^{1/6} R_0 \qquad (1)$$

derived for centrosymmetric QD donor−protein dye acceptor (or QD−peptide−dye) conjugates, where n is the number of dye acceptors attached to the same QD scaffold and R_0 is the Förster distance where FRET efficiency equals 50%. R_0 is expressed as[33]

$$R_0 = 9.78 \times 10^3 [\kappa^2 n^{-4} Q_D J(\lambda)]^{1/6} \qquad (2)$$

where n is the refractive index of the medium, Q_D is the PL quantum yield of the donor in the absence of acceptor, $J(\lambda)$ is the integral of the spectral overlap, and κ^2 is the dipole orientation factor. We use $\kappa^2 = 2/3$ corresponding to a random dipole orientation shown to be appropriate for our self-assembled QD−protein−dye and QD−peptide−dye conjugates, as detailed in our previous studies.[31,32] The experimental FRET efficiency E is calculated using the expression:

$$E = \frac{(F_D - F_{DA})}{F_D} \qquad (3)$$

where F_D and F_{DA} are, respectively, the fluorescence intensities of the donor alone and the donor in the presence of acceptor(s).[32] FRET efficiency was calculated from the QD PL quenching, taking into account direct acceptor excitation component from control acceptor only samples as described.[30−32,34,35] The FRET efficiency represents an average over all QD−peptide conjugates. However, all QDs are not conjugated to the same number of acceptors. Instead, the number of labeled peptides per QD follows a Poisson distribution inherent to the self-assembly process. This usually has a negligible effect on the data analysis when the FRET efficiencies are small (<30−40% for an acceptor:QD ratio $n = 1$) and scale linearly with the number of acceptors per QD throughout the distribution width. We took this distribution into account in the data analysis with YEHK$_{1,3}$ where the FRET efficiencies at $n = 1$ are larger than

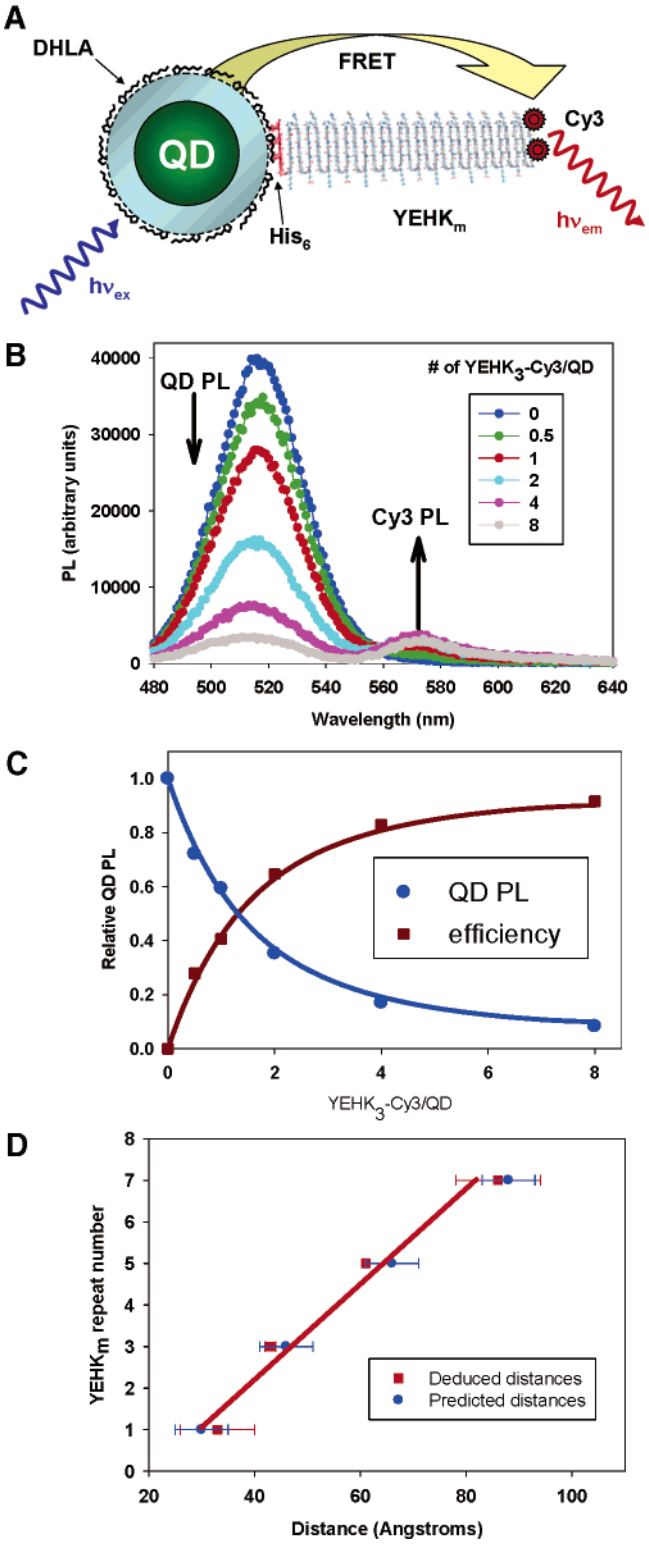

Figure 3. (A) Schematic representation of a QD−YEHK$_m$−Cy3 conjugate engaged in FRET interactions (one dye-labeled peptide per QD is shown for simplicity). (B) Composite PL emission spectra collected from conjugate solutions with YEHK$_3$−Cy3-to-QD ratios of 0, 0.5, 1, 2, 4, and 8. The small direct excitation contribution using YEHK$_1$–Cy3 control solution was taken into account in deriving FRET efficiencies. (C) Plot of the relative QD PL vs Cy3-to-QD ratio along with the corresponding FRET efficiencies. Similar data were measured for the other QD−peptide conjugates. See Supporting Information. (D) Plot of the peptide end-to-end size extracted from FRET efficiency using eq 1, along with the predicted sizes based on considering the sequence, β-sheet conformation, and dye-linker length.

50%. The values for the center-to-center distance r_n were compared to estimates derived by considering the structural characteristics of the system: centrosymmetric QD−YEHK$_m$ conjugate, QD radius, and assuming that all peptides have a β-strand conformation. The Y-to-Y residue distance in the repeats is estimated to be 9−10 Å.[22−27] An additional 1−1.5 Å is added for each additional YEHK repeat in a particular peptide due to bulk constraints.[18] The distance from the sulfurs on the cysteines to the Cy3 center is estimated as 7−9 Å.[30]

Surface Arrays of QDs and QD−Peptide/Protein Assemblies. Arrays of QDs and QD−bioconjugates were assembled on glass substrates using PDMS flow channels mounted on microscope glass slides (PDMS flow cell); see Supporting Information Figure 1. The PDMS flow cell is first clamped on the substrate and channels are filled with a first round of reagents in a functionalization step. After rinsing, the PDMS cell is dismounted, rotated 90°, and clamped on the substrate and the channels are filled with a second round of reagents (assay step). This allows selection of functional arrays (reactive squares) that can be tested optically and/or assayed. Additional details can be found in refs 15 and 16. Substrates were initially functionalized with either NeutrAvidin or PAH before peptide bridging and QD array buildup.

Patterning on NeutrAvidin-Functionalized Substrates. Surface functionalization with NeutrAvidin was carried out following the procedures described.[15,16] A microscope slide coated with NeutrAvidin was first assembled with a patterning PDMS flow cell, and the channels were exposed to solutions of biotinylated YEHK$_m$ (Bt−YEHK$_m$) at concentrations ranging from 0.1 to 10 μg/mL in 10 mM phosphate buffer + 150 mM NaCl + 0.05% Tween (PBST) and allowed to incubate overnight at 4 °C. After rinsing with PBST, the slide was assembled with the assay flow cell (rotated 90° with respect to the first one). Channels were then filled with QD solutions (530 nm QDs at 800 nM or 590 nm QDs at 400 nM) in borate buffer (10 mM pH 9.6) + Tween (0.05−1.0%) and allowed to incubate for 3 h at room temperature. Following rinsing with borate buffer the slide was either disassembled from the PDMS cell and imaged, or further incubated with a solution of RR-labeled peptide at 150 nM in borate buffer + 0.05% Tween for 2 h at room temperature. The patterned substrates were imaged using a total internal reflection system (NRL Array Biosensor), equipped with an argon ion laser (488 nm) for excitation and a CCD camera for fluorescence collection, as described.[15,16] Weak nonspecific interactions between non-biotinylated peptides and NeutrAvidin (on the substrate) were noted in some rare cases and resulted in subsequent capture of QDs. Nonetheless, the QD PL signal generated from these arrays was very small (at least ~3 times smaller) compared to those collected from samples using biotinylated peptides.

Surface-Immobilized Sensing Assemblies. A FRET-based QD−MBP−dye biosensor specific for maltose was assembled stepwise onto NeutrAvidin-functionalized microtiter plate wells. Bt−YEHK$_7$ peptide was first attached to the plate wells. After rinsing, the peptide-coated substrates were used to capture 510 nm QDs. The wells were then exposed to a solution of 100 nM of His-terminated MBP41C−Cy3 and allowed to incubate overnight, before washing with borate buffer. MBP41C−Cy3 designates an MBP mutant labeled at cysteine residue 41 with Cy3 dye. QD−MBP41C−Cy3 assemblies were tested by exposing the wells to various amounts of either soluble maltose or buffer control for 5 min. PL spectra were collected using the microtiter plate reader. Changes in the PL signature were then transformed into binding curves as described.[31,34]

Results

Polypeptide Design and Expression. The polypeptide sequences used in this study originate from the structure of β-sheet forming silk-like polypeptides[24,25] and consist of a variable number of core β-strand structures with tyrosine (Y), glutamic acid (E), histidine (H), and lysine (K) residues located at the turns. See Figure 1A,B for the sequence and structure. Due to this unique β-strand repeat sequence, the polypeptides form a rigid "rodlike" structure with the negatively charged glutamic acids and positively charged lysines at adjacent turns of the same edge contributing to the antiparallel structure by salt bridge formation.[22,23] This structure has been confirmed by spectroscopy and both atomic force and electron microscopy studies.[22−25] An essential element of the polypeptide design is the ability to introduce desired amino acid functionalities, not only along the β-sheet structure, but also at both termini of the sequence. Although several variants on the design have been created (see discussion), for the current series we utilize an N-terminal dicysteine and C-terminal hexahistidine (His$_6$) construct with the core "YEHK" unit repeated in blocks of either 2 (m = 1, 3, 5, 7) or 7 (m = 7, 14, 21, 28, 35), referred to hereon as YEHK$_m$, where m designates the specific number of core repeats. Figure 1C shows an SDS−PAGE gel of the purified YEHK$_m$ 7-repeat series. As the number of repeat units increases, so too does the molecular weight of the purified polypeptide, with the molecular weights (measured against the sizing ladder) in very good agreement with those predicted from the sequence.

Characterization of QD-YEHK$_m$ Peptide Assemblies in Solution. We have previously shown that appending terminal oligohistidine sequences (His$_6$) onto proteins can facilitate metal-affinity-driven self-assembly of such proteins onto CdSe−ZnS QDs capped with a solubilizing layer of DHLA.[30−32,35] This approach allows control over the protein-to-QD ratios and in some cases even protein orientation within the conjugate.[30,35] We have also shown that FRET interactions between QD and dye-labeled protein acceptors in these conjugates are well-described using Förster formalism and that accurate values for the center-to-center separation distances for these centrosymmetric conjugates can be measured using eq 1.[30,32,35]

FRET with QD donors offers four specific benefits not available when using conventional organic dyes or fluorescent proteins. These include the following proteins: (1) the ability to array multiple acceptors around a single QD to increase the overall FRET efficiency; (2) the possibility of exciting a QD population at any wavelength to the blue of its absorption band edge, which substantially reduces direct excitation of the acceptor; (3) the ability to tune the degree of spectral overlap (Förster distance, R_0) by changing the QD donor size/emission color to match a given dye acceptors' absorbance profile; (4) the ability to perform simultaneous or "multiplex" FRET experiments.[6,32,36,37] When combined, these benefits have allowed us to probe the structure and interactions of several proteins as they interact with QDs.[30,32,35,37] We first employed FRET between the QD donor and acceptor dye-labeled peptides to probe how the peptides configure themselves as they self-assemble onto the QD scaffolds and form QD−peptide conjugates. Figure 3A shows a putative schematic of this type of QD-YEHK$_m$ bioconjugate, where the QD is engaged in FRET with dyes attached at the peptides' distal cysteine residues. Figure 3B shows a representative composite set of PL spectra collected from 510 nm QDs incubated with an increasing ratio of YEHK$_3$–Cy3/QD. The corresponding FRET efficiency data shown as fractional QD PL loss and efficiency (1 − fractional

TABLE 1: Center-to-Center Separation Distances along with the End-to-End Peptide Extension *L* for the Various Systems Studied[a]

dye-labeled peptide used	donor QD, radius *a* (Å)	separation distance, *r* (Å)	peptide spatial extension, *L* (Å)
$YEHK_1$−Cy3	510 nm QD, 25−26	35 ± 3	10 ± 2
$YEHK_3$−Cy3	510 nm QD, 25−26	43 ± 1	18 ± 1
$YEHK_5$−Cy3	510 nm QD, 25−26	61 ± 1	35 ± 1
$YEHK_7$−Cy3	530 nm QD, 28−29	90 ± 8	62 ± 7

[a] Note: The *L* values include the dye linker.

QD PL) is shown in Figure 3C. Similar data were collected for the other YEHK polypeptides that repeated in blocks of 2 ($m = 1, 5, 7$); see Supporting Information Figure 2. A fit of the experimental FRET efficiency versus ratio n (using eq 1 and R_0 values of 46 Å for the 510 nm QD−Cy3 pair and 50.5 Å for the 530 nm QD−Cy3 pair) provided estimates of the average values of r_n for each of these conjugates (see Table 1).[32] Table 1 also shows the corresponding dye-labeled peptide end-to-end distance/size *L* extracted from such fits. For this we treated the QDs as spheres of average radius *a* (values extracted from structural characterization),[30−32] took into account the presence of two cysteines and thus 2 Cy3 dyes per peptide, and assumed that the His_6 tag is in close contact with the QD surface in an energy-minimized conformation.[30,32,35] This treatment also implies that the His tract and DHLA layer are highly interpenetrated and have minor contribution to the derived r_n values.[30] An additional 7−9 Å between the N-terminal cysteine−thiol and Cy3 is used in deriving the *L* values; it accounts for the spatial contribution of the dye-linker and maleimide functionality.[30]

Several salient features can be derived from this analysis. The rather small *L* value extracted for peptide $YEHK_1$ is a clear reflection of the high FRET efficiency measured for this set, where near unity is reached for $n = 2$. However, for the set of QD−$YEHK_7$ conjugates, the measured FRET efficiencies are low, due to the rather large separation distances involved (approaching $\sim 2R_0$). Overall, for this series of peptides ($m = 1,3,5,7$), the size *L* increases linearly with the number of repeat β-units in the sequence and correlates well with the predicted structure of these peptides in a rigid β-sheet configuration (Figure 3D). For example, without any structure and in a linear "end-to-end" arrangement, the $YEHK_7$ polypeptide is predicted to exceed 700 Å in length, which is reduced to around 350 Å on assumption of an α-helical structure and subsequently to ca. 55−65 Å in a β-sheet/turn conformation. We derive an *L* value of 62 ± 7 Å, which is in excellent agreement with the predicted β-sheet size.[18] *L* values for the longer peptide series ($YEHK_{14,21,28,35}$) could not be determined as r_n values were all larger than $2R_0$. This was not unexpected as the proteins should increase ∼50−60 Å in length with the addition of each block of 7 YEHK repeats. However, this does indicate that these longer polypeptides assemble on the QD surface via the His_6 tract and remain extended (rodlike) without collapsing onto the QD, reflecting their persistence length. It is also important to note that the above analysis indicates that the lone exposed histidines in the alternating $YEHK_m$ turn sequences do not interact with the QD. That interaction would significantly alter the FRET results by allowing the β-sheets to wrap themselves around the QD surface. Polyhistidine−metal affinity is driven by at minimum divalent interactions, and the lone histidine residues in the repeat sequence appear to be separated by enough distance to preclude this.[38,39]

As demonstrated in our previous studies using several His-appended proteins,[31,40] we also measured an enhancement in the PL of these QD−peptide conjugates (compared to unconjugated QDs) as a function of increasing unlabeled peptide-to-QD ratio; see Supporting Information Figure 3. The PL plateaus at higher ratios, corresponding to and indicating saturation in the protein packing around each QD.[19,31] This PL enhancement has been attributed to better passivation of the DHLA-capped QD surface due to interactions with the polyhistidine tract.[19,31,41,42] QD−peptide self-assembly was also monitored in the presence of imidazole, which disrupts this interaction (see Supporting Information Figure 3A,B). Imidazole is a structural mimic of the aromatic moiety on the histidine residues and competes for coordination to metals, thus its specific use as the eluting reagent during metal-affinity-based purification of oligohistidine-tagged proteins.[38,39] We found that enhancement in the solution PL of the QD−$YEHK_m$ conjugates was substantially smaller in the presence of the imidazole competitor. These results, in combination with the above FRET analysis, prove that the terminal His_6 on the peptides drives the interaction and self-assembly with the DHLA-capped QDs, resulting in consistent conjugate configuration with the N-terminal dicysteines facing the surrounding solution. Moreover, the FRET analysis indicates a level of control over the number of peptides assembled per QD.

Surface Immobilization of QDs using YEHK Peptides. We next explored the utility of these peptides for surface immobilization or tethering of QDs and QD−conjugates. Substrates functionalized with NeutrAvidin were exposed (in patterns) stepwise to the biotin-labeled 7-repeat $YEHK_m$ series ($m = 7$, 14, 21, 28, 35), rinsed with buffer, incubated with a solution of DHLA-capped QDs, rinsed, and then imaged as described in the Experimental Section; see Figure 4B. Peptide solutions at two different concentrations (10 and 1 μg/mL) were used for each series, whereas the QD concentration in solution was fixed but contained varying amounts of Tween-20. The fluorescence image collected from these substrates clearly shows that QDs are specifically captured by every peptide in the series, independent of length, and that the capture efficiency depends on the peptide concentration in the solution used; lower concentration resulted in weaker fluorescence (compare side-by-side columns in Figure 4B). No fluorescence was collected from the no-peptide control columns. These results also confirm that the His_6 residues are available for QD capture in this tethered configuration. Figure 4B also shows that capture efficiency decreases in the presence of Tween, with no QD signal measured at concentrations exceeding 0.5%. Similar results were found for patterns precoated with biotin−$YEHK_5$ polypeptide (see Supporting Information Figure 3C). To further test the effects of peptide density on the surface capture efficiency of QDs, Bt−$YEHK_7$ concentration was varied (ranging between 0.1 and 10 μg/mL), followed by channel incubation with a solution of QDs; see Figure 4C. A plot of the net QD fluorescence intensity (collected from each square and background-corrected) versus peptide concentration used is shown in Figure 4D. The data clearly show that capture efficiency is proportional to the peptide concentration used, illustrating the dose−response nature of both the biotin−NeutrAvidin interactions and the metal−His affinity between the peptide and QD surface; higher peptide density results in higher capture efficiency until saturation is reached. Furthermore, an examination of the figures shows little to no nonspecific interaction is apparent with these conditions, demonstrating control over any other interactions.

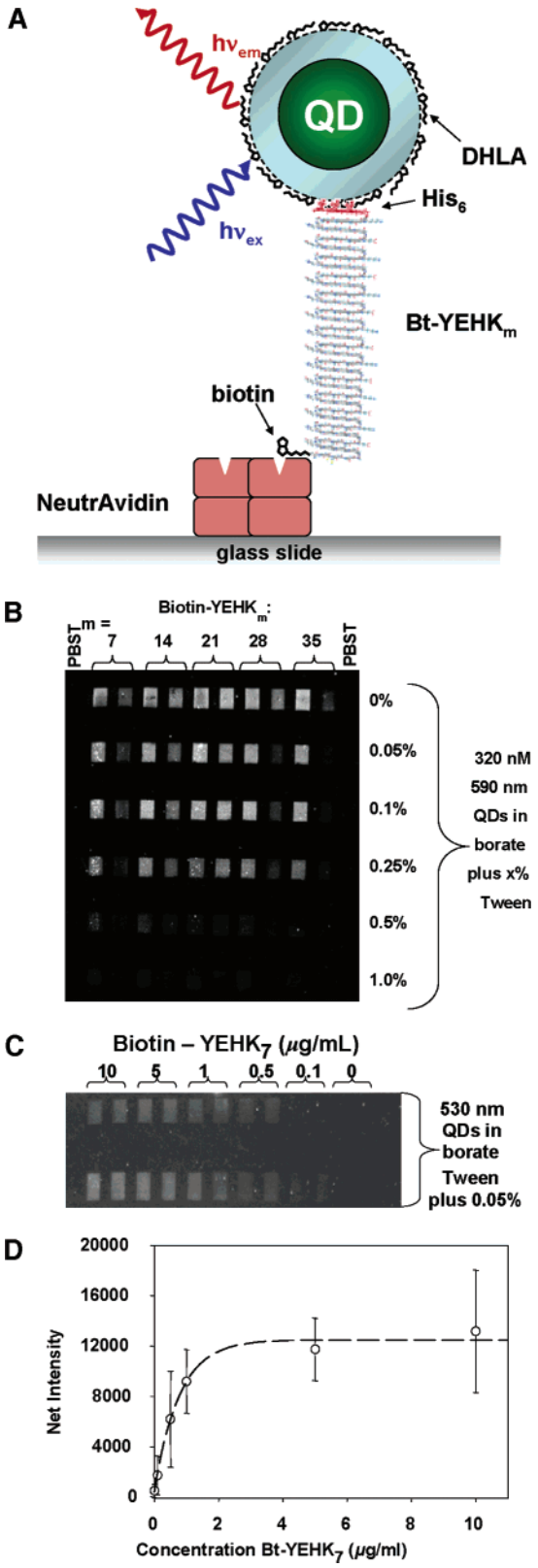

Figure 4. (A) Schematic representation of QD immobilization onto NeutrAvidin-functionalized substrate via a biotin−YEHK$_m$ (Bt−YEHK$_m$) bridge. (B) Fluorescence image (590 nm QD emission) collected of a pattern assembled using the 7-repeat biotinylated YEHK$_m$ series (7, 14, 21, 28, 35) at two peptide concentrations (10 and 1 μg/mL) in the presence of increasing concentrations of Tween detergent. Array was excited at 488 nm. (C) Image of 530 nm QDs immobilized onto NeutrAvidin waveguides functionalized with decreasing concentrations of the Bt−YEHK$_7$. (D) Plot of the QD intensity (background-subtracted) in C vs concentration of Bt−YEHK$_7$ in the initial peptide solutions used to pattern the waveguide prior to incubation with QDs.

Multifunctional YEHK−QD Arrays. Confident in the ability of YEHK$_m$ polypeptides to discretely capture QDs on surfaces, we investigated their ability to further capture a second layer of peptides/proteins and build other 2- and 3D QD arrays. In the first example, the above structure, consisting of NeutrAvidin−Bt−YEHK$_{14,21}$−QD, was incubated with a solution of RR-labeled YEHK$_7$ peptide (schematic in Figure 5A). Fluorescence images from these substrates were collected using 515 and 570 nm long-pass (LP) emission filters; these filters allow selection of the composite QD−RR dye signal or the RR dye only emission, respectively. Images shown in Figure 5B clearly show that RR emission was detected only in areas that were preincubated with DHLA-capped QDs, which confirm that the His−peptide−QD specific interactions can also be utilized to create an upper layer of oppositely oriented peptide. Interestingly, the RR excitation results from a combination of FRET from the 530 nm QDs and some weak direct laser excitation contribution (absorption of RR at 488 nm is low; see Figure 2). This corroborates our previous results on surface tethering of QDs which used proteins instead of peptides.[15] Similar results were obtained using PAH-functionalized substrates; in this case capture of QDs is driven by electrostatic interactions between the charges on the DHLA ligands and the layer of PAH on the surface (see Supporting Information Figure 4). This also demonstrates that similar structures can be created without reliance on NeutrAvidin-patterned waveguides or use of biotin−avidin interactions.

To demonstrate a more active use for these peptide materials in more complex structures, we took a previously developed solution-phase reagentless FRET biosensor for the nutrient maltose[34] and utilized the Bt−YEHK$_7$ protein to immobilize this QD-based biosensor to NeutrAvidin-coated microtiter well plates. A schematic of the sensor is shown in Figure 6A. Bt−YEHK$_7$ was used to immobilize 510 nm emitting QDs onto the NeutrAvidin-coated wells, and the nascent assembly was then exposed to maltose binding protein (MBP) specifically labeled on residue 41 with Cy3 (MBP41C−Cy3). Assembly of the MBP41C−Cy3 onto the upper surface of the QDs is again driven by MBP−His$_5$−Zn metal affinity coordination and brings the acceptor dye into close proximity of the QD donor resulting in efficient FRET between the two. Upon binding maltose, MBP undergoes an obligatory conformational change that alters the environment around the dye and results in a concentration-dependent change in dye emission. Changes in Cy3 emission are monitored while QD donor FRET "drives" the sensor since it is excited via the QD at a Cy3 absorption minimum.[34] The resulting change, derived from loss of MBP41C−Cy3 fluorescence, is plotted as a function of maltose concentration in Figure 6B. A limit of detection (LOD) of ~1 mM with an apparent dissociation constant (K_{app}) of 7.5 ± 1.6 mM maltose was derived. Several differences were noted when comparing this tethered sensor to the previous solution-phase prototype,[34] including a higher LOD and a smaller dynamic change in Cy3 emission upon maltose titration. These differences are most probably attributable to steric hindrance and packing constraints imposed on the surface-tethered dye-labeled MBP. Furthermore, only the upper exposed surfaces of the QDs are probably available for MBP41C−Cy3 functionalization. Nevertheless, this represents a promising strategy for preparing surface-immobilized QD−protein sensors. Last, as another demonstration of the versatility afforded by these peptides, we utilized their His$_6$ functionality to attach a YEHK$_7$−RR protein to a Ni^{2+} chelate modified surface in a "flipped" configuration (see Supporting Information Figure 4).

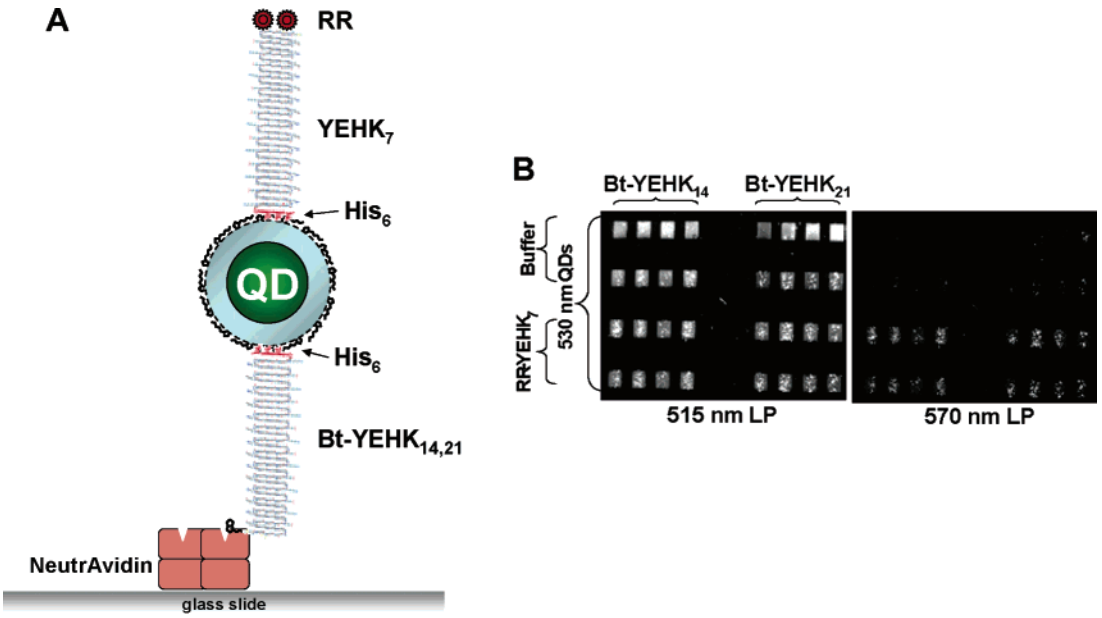

Figure 5. (A) Schematic representation of surface assembly. NeutrAvidin-functionalized substrates are first incubated with Bt−$YEHK_{14,21}$ followed by incubation with 530 nm emitting QDs and then a solution of $YEHK_7$−RR or buffer to allow QD−$YEHK_7$−RR assembly. (B) Fluorescent image collected using 515 and 570 nm long-pass filters. Only areas incubated with $YEHK_7$−RR emit signal when measured with the 570 LP filter.

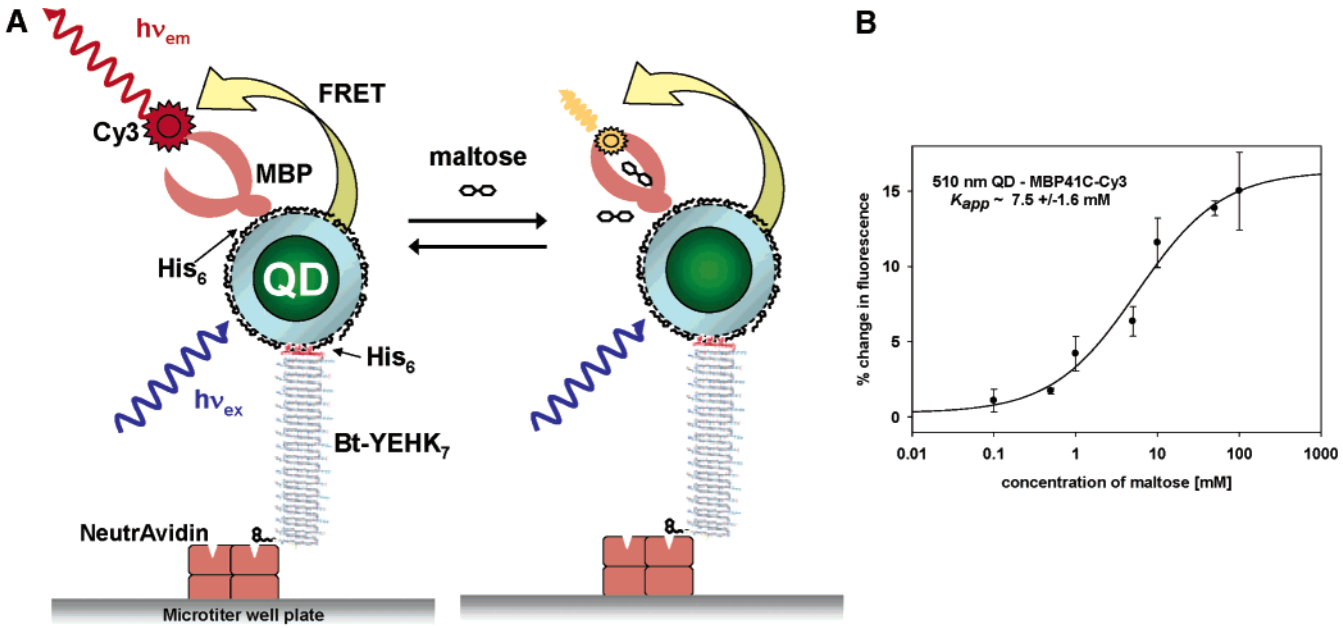

Figure 6. (A) Schematic of a FRET-based surface-immobilized maltose biosensor. QDs emitting at 510 nm were captured in NeutrAvidin-coated microtiter well plates functionalized with biotin-labeled $YEHK_7$. The immobilized QDs are further self-assembled with a mutant dye-labeled maltose binding protein, MBP41C−Cy3. Upon addition of maltose, the MBP41C−Cy3 undergoes a conformational change altering the environment around the dye and its emission.[34] (B) Saturation curve for the surface-immobilized maltose biosensor. The change in Cy3 emission (loss of fluorescence) is plotted vs maltose concentration. The K_{app} value was derived from the average of three titrations.

Discussion and Conclusions

In this report we utilized a combination of electrophoresis, FRET, biotin−avidin chemistry, self-assembly, and UV−vis fluorometry to probe and gain insight into the structure of the YEHK peptides, their interactions with QDs, and their self-assembly into complex functional nanostructures. The YEHK peptide series is monodisperse and rigid with specific functionalities at both their N- and C-termini. This allows them to act as bridges that tether the QDs to surface-modified substrates. The tethering method, driven by self-assembly, is simple and reproducible and does not rely on chemical modification of the nanoparticle surface. We have shown that these His-terminated peptides can self-assemble onto DHLA-capped QDs in solution, with reasonable control of peptide-to-QD ratios. We have also demonstrated that biotin-functionalized peptides could be easily attached onto NeutrAvidin-functionalized substrates and serve as bridges for surface tethering of QDs and QD−peptide/QD−protein assemblies. Key criteria were incorporated into the polypeptides design. Foremost, is the ability to reconfigure peptide sequence, structure, size, or flanking motif(s) using recombinant engineering. Although the current series has flanking polyhistidine and dicysteine sequences, a number of variants have been created including peptides with only His_6 flanking regions and even a His_6/Cys_6 construct. These flanking sequences have been purposely kept as a variable architecture in the design so as to allow targeted interactions with similar

or disparate materials/nanoparticles. For example the His_6 motif will coordinate to Cu, Co, Ni, Zn, Mn, Fe, and Cr, while the cysteine−thiols will bind to Au, Ag, S, Pt, and Pd as well as other metals.[4,5,38,39] The number of cysteine, histidine, or other residues at the termini can be tailored to adjust binding affinity or provide different functionalities. For example, monocysteine constructs will provide a single site for a fluorophore, biotin, or other desired thiol-based modification.

Another important design criterion is control over length. Each polypeptide series is uniform with variation only in the length, provided by varying the repeat number. A specifically desired repeat size/length peptide in the 1−50 repeat range can easily be created, selected for, and expressed. Moreover, the residues utilized in the β-strand repeat maintain a stable, defined rodlike structure. Control over size is highlighted by the ability to place a series of dyes within predetermined distances from the QD surface using the $YEHK_{1,3,5,7}$ series. Although not characterized in this study, we expect that the control over distance may be maintained for the entire $YEHK_m$ series used. This feature will be important to future designs which may incorporate fixed lengths between surface(s) and dye(s)/nanoparticle(s) or even multilayered structures. For example, such configurations may allow studies of distance dependence on noble metal−fluorescent dye enhancement.[43] A further consideration is found in the type and location of residues used in at the β-turn. The glutamic acid−lysine salt bridge provides stability, while the tyrosines may allow exploration of electron tunneling dynamics.[44] Other variants on this design with YEYK or KYEY repeats have been created to align tyrosine residues for this. For such electronic experiments the plasticity of both length and design will again be important and may allow self-assembly across nanoscale metallic electrodes. Polypeptides or series of polypeptides are produced in milligram quantities, and the bacterial expression system can be scaled to allow production of large amounts. Although quite effective for discretely immobilizing QDs on surfaces, the potential uses of these polypeptides remain largely unexplored, and we believe that these materials may provide versatile building blocks suitable for controlled nanoscale interactions with both QDs/nanoparticles and surfaces.

Acknowledgment. The authors acknowledge NRL and L. Chrisey at the Office of Naval Research (ONR Grant No. N001404WX20270) for support. A.R.C is supported by a National Research Council Fellowship through NRL. T.P. acknowledges a postdoctoral fellowship from the Fondation pour la Recherche Medicale (France). J.T.W. and S.H. acknowledge the Microelectronics Advanced Research Corp. (MARCO), DARPA, and the New York State Office of Science, Technology and Academic Research (NYSTAR) through the Interconnect Focus Center (IFC) and the Materials, Structures, and Devices (MSD) Center.

Supporting Information Available: Schematics of the patterning and assay PDMS, the NRL array biosensor, imidazole competition assays, PAH patterning of QDs, and FRET titrations. This information is available free of charges via the Internet at http://pubs.acs.org.

References and Notes

(1) Niemeyer, C. M. *Angew. Chem., Int. Ed.* **2001**, *40*, 4128.
(2) Niemeyer, C. M. *Angew. Chem., Int. Ed.* **2003**, *42*, 5796.
(3) Burda, C.; Chen, X. B.; Narayanan, R.; El-Sayed, M. A. *Chem. Rev.* **2005**, *105*, 1025.
(4) Daniel, M. C.; Astruc, D. *Chem. Rev.* **2004**, *104*, 293.
(5) Katz, E.; Willner, I. *Angew. Chem., Int. Ed.* **2004**, *43*, 6042.
(6) Medintz, I.; Uyeda, H.; Goldman, E.; Mattoussi, H. *Nat. Mater.* **2005**, *4*, 435.
(7) Michalet, X.; Pinaud, F. F.; Bentolila, L. A.; Tsay, J. M.; Doose, S.; Li, J. J.; Sundaresan, G.; Wu, A. M.; Gambhir, S. S.; Weiss, S. *Science* **2005**, *307*, 538.
(8) Zhang, C. L.; Xu, T.; Butterfield, D.; Misner, M. J.; Ryu, D. Y.; Emrick, T.; Russell, T. P. *Nano Lett.* **2005**, *5*, 357.
(9) Cui, Y.; Bjork, M.; Liddle, A.; Sonnichsen, C.; Boussert, B.; Alivisatos, P. *Nano Lett.* **2004**, *4*, 1093.
(10) Zhou, D. J.; Bruckbauer, A.; Abell, C.; Klenerman, D.; Kang, D. J. *Adv. Mater.* **2005**, *17*, 1243.
(11) Wu, X. C.; Bittner, A. M.; Kern, K. *Adv. Mater.* **2004**, *16*, 413.
(12) Hens, Z.; Talapin, D. V.; Weller, H.; Vanmaekelbergh, D. *Appl. Phys. Lett.* **2002**, *81*, 4245.
(13) Baumle, M.; Stamou, D.; Segura, J.-M.; Hovius, R.; Vogel, H. *Langmuir* **2004**, *20*, 3828.
(14) Constantine, C. A.; Gattas-Asfura, K. M.; Mello, S. V.; Crespo, G.; Rastogi, V.; Cheng, T. C.; De Frank, J. J.; Leblanc, R. M. *J. Phys. Chem. B* **2003**, *107*, 13762.
(15) Sapsford, K. E.; Medintz, I. L.; Golden, J. P.; Deschamps, J. R.; Uyeda, H. T.; Mattoussi, H. *Langmuir* **2004**, *20*, 7720.
(16) Medintz, I. L.; Sapsford, K. E.; Konnert, J. H.; Chatterji, A.; Lin, T. W.; Johnson, J. E.; Mattoussi, H. *Langmuir* **2005**, *21*, 5501.
(17) Portney, N. G.; Singh, K.; Chaudhary, S.; Destito, G.; Schneemann, A.; Manchester, M.; Ozkan, M. *Langmuir* **2005**, *21*, 2098.
(18) Lewin, B. *Genes IV*, 4th ed.; Oxford University Press: New York, 1990.
(19) Mattoussi, H.; Mauro, J. M.; Goldman, E. R.; Anderson, G. P.; Sundar, V. C.; Mikulec, F. V.; Bawendi, M. G. *J. Am. Chem. Soc.* **2000**, *122*, 12142.
(20) Murray, C. B.; Norris, D. J.; Bawendi, M. G. *J. Am. Chem. Soc.* **1993**, *115*, 8706.
(21) Peng, Z. A.; Peng, X. *J. Am. Chem. Soc.* **2001**, *123*, 183.
(22) Topilina, N. I.; Higashiya, S.; Rana, N.; Ermolenkov, V. V.; Kossow, C.; Carlsen, A.; Ngo, S. C.; Wells, C. C.; Eisenbraun, E. T.; Dunn, K. A.; Lednev, I. K.; Geer, R. E.; Kaloyeros, A. E.; Welch, J. T. *Biomacromolecules* **2006**, *7*, 1004.
(23) Higashiya, S.; Ngo, S. C.; Bousman, K. S.; Welch, J. T.; Rana, N.; Carlsen, A.; Eisenbraun, E. T.; Geer, R. E.; Kaloyeros, A. E. *ACS Prepr. Polym. Mater. Sci. Eng.* **2003**, *89*, 322.
(24) Yoshikawa, E.; Fournier, M. J.; Mason, T. L.; Tirrell, D. A. *Macromolecules* **1994**, *27*, 5471.
(25) McGrath, K. P.; Fournier, M. J.; Mason, T. L.; Tirrell, D. A. *J. Am. Chem. Soc.* **1992**, *114*, 727.
(26) McPherson, D. T.; Xu, J.; Urry, D. W. *Protein Expression Purif.* **1996**, *7*, 51.
(27) Cantor, E. J.; Atkins, E. D. T.; Cooper, S. J.; Fournier, M. J.; Mason, T. L.; Tirrell, D. A. *J. Biochem.* **1997**, *122*, 2217.
(28) Medintz, I. L.; Goldman, E. R.; Lassman, M. E.; Mauro, J. M. *Bioconjugate Chem.* **2003**, *14*, 909.
(29) *Bioconjugate Techniques*; Hermanson, G. T., Ed.; Academic Press: San Diego, 1996.
(30) Medintz, I. L.; Konnert, J. H.; Clapp, A. R.; Stanish, I.; Twigg, M. E.; Mattoussi, H.; Mauro, J. M.; Deschamps, J. R. *Proc. Natl. Acad. Sci. U.S.A.* **2004**, *101*, 9612.
(31) Medintz, I. L.; Clapp, A. R.; Mattoussi, H.; Goldman, E. R.; Fisher, B.; Mauro, J. M. *Nat. Mater.* **2003**, *2*, 630.
(32) Clapp, A. R.; Medintz, I. L.; Mauro, J. M.; Fisher, B. R.; Bawendi, M. G.; Mattoussi, H. *J. Am. Chem. Soc.* **2004**, *126*, 301.
(33) Lakowicz, J. R. *Principles of Fluorescence Spectroscopy*, 2nd ed.; Kluwer Academic/Plenum: New York, 1999.
(34) Medintz, I. L.; Clapp, A. R.; Melinger, J. S.; Deschamps, J. R.; Mattoussi, H. *Adv. Mater.* **2005**, *17*, 2450.
(35) Goldman, E.; Medintz, I.; Whitley, J.; Hayhurst, A.; Clapp, A.; Uyeda, H.; Deschamps, J.; Lassman, M.; Mattoussi, H. *J. Am. Chem. Soc.* **2005**, *127*, 6744.
(36) Clapp, A. R.; Medintz, I. L.; Mattoussi, H. *ChemPhysChem* **2006**, *7*, 47.
(37) Clapp, A. R.; Medintz, I. L.; Uyeda, H. T.; Fisher, B. R.; Goldman, E. R.; Bawendi, M. G.; Mattoussi, H. *J. Am. Chem. Soc.* **2005**, *127*, 18212.
(38) Ueda, E. K. M.; Gout, P. W.; Morganti, L. *J. Chromatogr., A* **2003**, *988*, 1.
(39) Hainfeld, J. F.; Liu, W.; Halsey, C., M. R.; Freimuth, P.; Powell, R., D. *J. Struct. Biol.* **1999**, *127*, 185.
(40) Goldman, E. R.; Medintz, I. L.; Hayhurst, A.; Anderson, G. P.; Mauro, J. M.; Iverson, B. L.; Georgiou, G.; Mattoussi, H. *Anal. Chim. Acta* **2005**, *534*, 63.
(41) Mamedova, N. N.; Kotov, N. A.; Rogach, A. L.; Studer, J. *Nano Lett.* **2001**, *1*, 281.
(42) Hanaki, K.; Momo, A.; Oku, T.; Komoto, A.; Maenosono, S.; Yamaguchi, Y.; Yamamoto, K. *Biochem. Biophys. Res. Commun.* **2003**, *302*, 496.
(43) Stranik, O.; McEvoy, H. M.; McDonagh, C.; MacCraith, B. D. *Sens. Actuators, B* **2005**, *107*, 148.
(44) Kappler, U.; Bailey, S. *J. Biol. Chem.* **2005**, *280*, 24999.